

## PHYSICS

## Strongly interacting dipolar-polaritons

Itamar Rosenberg<sup>1</sup>, Dror Liran<sup>1</sup>, Yotam Mazuz-Harpaz<sup>1</sup>, Kenneth West<sup>2</sup>, Loren Pfeiffer<sup>2</sup>, Ronen Rapaport<sup>1,3\*</sup>

Exciton-polaritons are mutually interacting quantum hybridizations of confined photons and electronic excitations. Here, we demonstrate a system of optically guided, electrically polarized exciton-polaritons (“dipolaritons”) that displays up to 200-fold enhancement of the polariton-polariton interaction strength compared to unpolarized polaritons. The magnitude of the dipolar interaction enhancement can be turned on and off and can be easily tuned over a very wide range by varying the applied polarizing electric field. The large interaction strengths and the very long propagation distances of these fully guided dipolaritons open up new opportunities for realizing complex quantum circuitry and quantum simulators, as well as topological states based on exciton-polaritons, for which the interactions between polaritons need to be large and spatially or temporally controlled. The results also raise fundamental questions on the origin of these large enhancements.

## INTRODUCTION

Exciton-polaritons are quantum superposition states (quasiparticles) of optically confined light and electronically confined excitations (excitons) in semiconductor quantum structures. Polaritons have very low effective masses due to their photonic part and substantial particle interactions due to their excitonic part. This combination of properties has yielded observations on many collective quantum phenomena (1–10), and it makes polaritons appealing for developing nonlinear optical components on the quantum level. It has been recently suggested theoretically that quantum simulators, similar to those demonstrated with cold atoms, can be constructed using quantum condensates of exciton-polaritons in lattices (11, 12). Furthermore, recent demonstrations of low-loss, high-velocity slab-waveguided exciton-polaritons (13–16) have opened up possibilities for demonstrating real functional polariton-based quantum circuitry on an optical chip, in a parallel effort to the one based on Rydberg atoms (17–21), and to realize interacting topological polaritons (“topolaritons”) as was suggested recently (22).

Major efforts are on the way toward a realization of proposals for quantum devices using polaritons; however, the main obstacle for realizing these quantum systems is that they usually require strong interactions between only two polaritons, which is necessary to achieve entanglement and logic operations for quantum circuitry, and sufficient on-site interactions for quantum lattice simulators. Because the interactions between polaritons stem from the excitonic part of the quasiparticles and because excitons are neutral, unpolarized particles, these interactions are rather weak and short ranged; thus, one needs to squeeze polaritons into very tiny, deep submicrometer areas to achieve sufficiently strong interactions. This squeezing of optical waves is a difficult challenge; thus, only classical optical simulators and nonlinear polariton effects involving many particles have been demonstrated to date. Furthermore, unlike in atomic systems, where interactions can be tuned effectively, the interaction strength in current polariton systems is completely determined by the system parameters and therefore cannot be controlled externally, either in time or space. These fixed interactions may strongly limit applications where external control and tuning of the interaction strength is necessary [we note here that a recent study reported evidence for interactions between unpolarized polaritons (23), which is much larger than previous reports].

On the other hand, it is by now well established that while neutral unpolarized excitons interact weakly, excitons that carry an electric dipole moment (sometimes known as dipolar excitons) display much larger interactions, manifested by very large energy blue shifts of their emission line, and large collisional broadening (24–26). These interactions stem from the long-range dipole-dipole interactions,  $V_{dd}(r) \approx e^2 d^2 / (\epsilon r^3)$ , rather than the contact exchange interactions of unpolarized excitons, thus significantly increasing the scattering cross section, as is evident by recent observations of dipolar spatial correlations of dipolar excitons (24–26), dipolar blockade between ensembles (27), and between only two excitons (28). Adopting dipolar interactions into polariton systems by realizing dipolar-polaritons could bridge the “interaction gap” of current polariton systems. However, dipolar excitons are usually realized with the electron and the hole separated into two adjacent quantum wells (QWs; a double QW geometry), which diminish their coupling to light and thus inhibit strong coupling and the formation of polaritons. Therefore, realizing dipolaritons with a double QW structure is very challenging (29).

Recently, we have shown that slab-waveguide (WG) dipolaritons can be realized with a heterostructure containing only single QWs, circumventing the strong coupling challenge and allowing a full electrical control of the electric dipole moment of the polaritons (15). Here, we demonstrate a system of optically guided, low-loss, electrically polarized exciton-dipolaritons with an electrically tunable dipole moment. We show compelling evidence for a large enhancement of the interaction strength between dipolaritons compared to unpolarized polaritons. The dipolar nature of the interaction is demonstrated through the linear dependence of the energy blue shifts of the polariton signal and the quadratic dependence of the polariton-polariton scattering rate on the dipole size. The magnitude of the dipolar interaction enhancement can be easily controlled over a very wide range by varying the applied polarizing electric field. The measured interaction strengths are shown to be in the range required for realistic two-polariton gates. This finding, together with the very long propagation distances of these dipolaritons, can open up new opportunities for realizing quantum circuitry based on exciton-polaritons.

## EXPERIMENTAL RESULTS AND MODELING

## Experimental concept

The sample structure and the experimental method are plotted in Fig. 1A. The sample is constructed in a WG geometry to support guided polariton modes, made of waveguided photons strongly interacting

Copyright © 2018  
The Authors, some  
rights reserved;  
exclusive licensee  
American Association  
for the Advancement  
of Science. No claim to  
original U.S. Government  
Works. Distributed  
under a Creative  
Commons Attribution  
NonCommercial  
License 4.0 (CC BY-NC).

<sup>1</sup>Racah Institute of Physics, The Hebrew University of Jerusalem, Jerusalem 91904, Israel. <sup>2</sup>Department of Electrical Engineering, Princeton University, Princeton, NJ 08544, USA. <sup>3</sup>Applied Physics Department, The Hebrew University of Jerusalem, Jerusalem 91904, Israel.

\*Corresponding author. Email: ronennr@phys.huji.ac.il

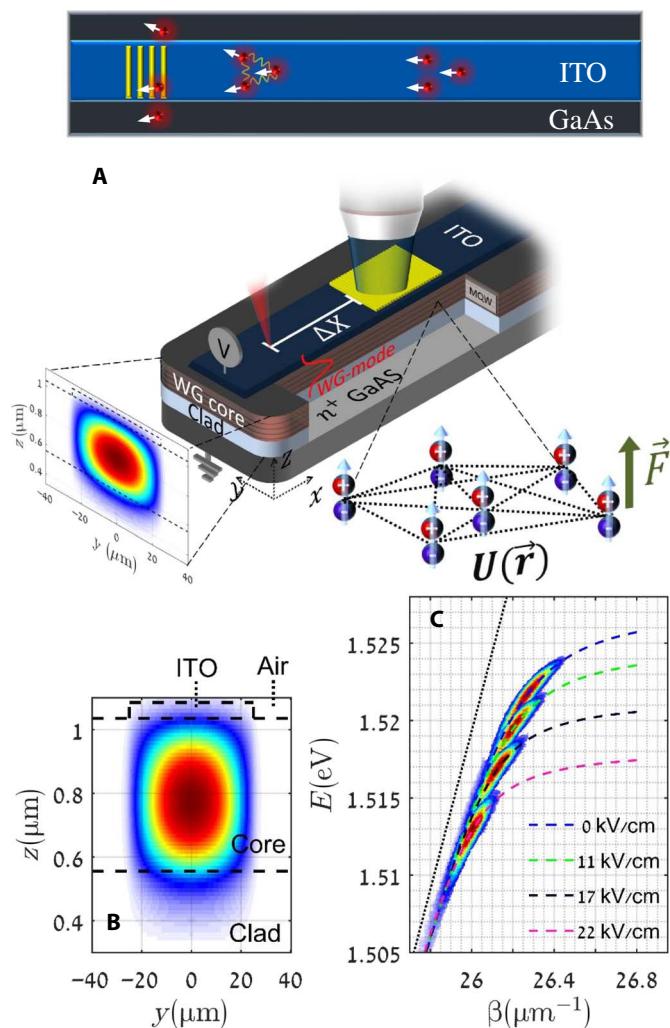


**Fig. 1. Electrically polarized WG-polaritons with mutual dipole-dipole interactions.** (A) Illustration of the system, sample, and the experimental method. Top: Schematic illustration of electrically polarized WG exciton-polaritons propagating inside an optical WG structure and of the dipole-dipole interaction and scattering of polaritons that can lead to energy shifts and propagation losses inside the WG. Bottom: Sample structure and experimental method: A nonresonant excitation through a thin ITO channel is used to excite confined polaritons, which propagate along the WG channel with a propagation constant  $\beta$ . A gold grating coupler with a periodicity of 240 nm located  $\Delta X$  from the excitation spot is used to couple the signal out into the acquisition system. When a voltage is applied to the channel, the polaritons become electrically polarized, acquiring a dipole moment. Polaritons then interact with each other via dipole-dipole interactions. MQW, multiple QW. (B) Calculated field distribution of the first WG mode confined by the ridge WG structure. (C) Overlaid photoluminescence (PL) measured at four different values of  $F$ , all fitted to the coupled oscillator model. The black dotted line is the bare photon mode. The red shift of the dispersion is a result of the quantum-confined Stark shift that polarizes the excitons (full images of all the four corresponding dispersions can be found in the Supplementary Materials).

with excitonic transitions of a set of twelve 20-nm-thick QWs positioned inside the WG core. [The core of the optical WG consists of a set of twelve 20-nm-thick  $\text{Al}_{0.4}\text{Ga}_{0.6}\text{As}/\text{GaAs}/\text{Al}_{0.4}\text{Ga}_{0.6}\text{As}$  QWs and a 500-nm bottom clad layer made of  $\text{Al}_{0.8}\text{Ga}_{0.2}\text{As}$ . See the study of Rosenberg *et al.* (15) for the details of the sample structure.] The top clad layer is made of a deposited 50-nm-thick, 50- $\mu\text{m}$ -wide transparent and conductive

indium tin oxide (ITO) channel. This ITO channel defines a ridge WG structure, supporting guided modes that are confined both vertically and laterally, yielding two-dimensional optical confinement for the polaritons, as depicted in Fig. 1B. The ITO layer also serves as a top electrode, to which voltage can be applied with respect to the  $n^+$ -doped GaAs back gate, resulting in a constant electric field ( $F$ ) directed perpendicularly to the QWs' plane (see Fig. 1A). The electric field induces a quadratic Stark energy red shift of the exciton resonance (30), leading to a red shift of all the polaritonic branches at the anti-crossing point. Furthermore, the applied field induces a polarization of the electron and hole wave functions along the  $z$  direction, resulting in a net electric dipole moment of the excitons and thus of the WG-polaritons (15). Both the energy of the WG-polaritons and their dipole moment are controlled by the applied field. Our experiments, carried out at a sample temperature of  $\sim 5$  K, use the fact that the propagation velocity of waveguided polaritons is four orders of magnitude larger than the typical propagation velocity of dipolar excitons (30  $\mu\text{m}/\text{ps}$  for the polaritons compared to 1 to 10  $\mu\text{m}/\text{ns}$  for excitons) (31, 32). This fact offers a “built-in” mechanism to separate the polaritons from the exciton cloud: At each measurement, our focused laser pulse ( $\lambda = 774.5$  nm; duration  $\approx 280$  ps) excites WG-polaritons that propagate along the WG from a specific distance  $\Delta X$  toward a metallic grating that couples the guided polariton signal out to the measuring optical system. The pulse is synchronized with a 10-ns exposure window of a gated intensified charge-coupled device (ICCD) camera (PI-MAX), which images the emission in the Fourier plane of the grating outcoupler, thus recording the angular-resolved dispersion of the signal emitted from the readout area. With typical  $\Delta X$  values ranging from tens to hundreds of micrometers, this type of remote excitation scheme separates the populations of the fast polaritons from that of the slow-moving excitons or charges and thus guarantees that only polaritons are present at the measurement area during the  $\sim 300$  ps it takes the polariton cloud to pass through the output grating. To ensure no buildup of long-lived exciton or charge reservoirs between excitation pulses, in all experiments, we modulated and synchronized the voltage with the excitation pulse and the exposure window, and we turned off the voltage after every exposure until the next one (see Materials and Methods for more details on the experimental methods). Figure 1C shows a set of measured WG-polariton dispersions (showing the polariton energy versus  $\beta$ , the propagation wave vector of the polaritons) under various applied electric fields  $F$ . The effect of the Stark shift on the polaritonic dispersion is seen.

### Measurements of the interaction-induced polariton energy shifts

We now turn to investigate the impact of the induced electric dipole on the polariton-polariton interactions. This can be done by monitoring the changes in the polariton dispersion under variations of the polariton densities (controlled by the excitation power) and variations of the polariton electric dipole (controlled by the applied voltage). Initial evidence for induced dipolar polariton-polariton interactions can be seen in Fig. 2 (A to C). Here, we placed our excitation spot at a distance of  $\Delta X = 65$   $\mu\text{m}$  from the grating outcoupler under different excitation powers and for different values of  $F$ . Figure 2 (A to C) shows overlaid measured polariton dispersions acquired for two excitation powers (low and high) for three different values of  $F$ . Because the bare exciton energy and thus the polariton energy red shift with increasing  $F$  and because we want to plot all dispersions on the same energy scale, we used an energy scale relative to the bare exciton energy,  $\delta E(F) = E - E_x(F)$ .

While there is only a tiny energy blue shift of the dispersion when  $F = 0$  (Fig. 2A), it can be seen that the polaritonic dispersion blue shifts

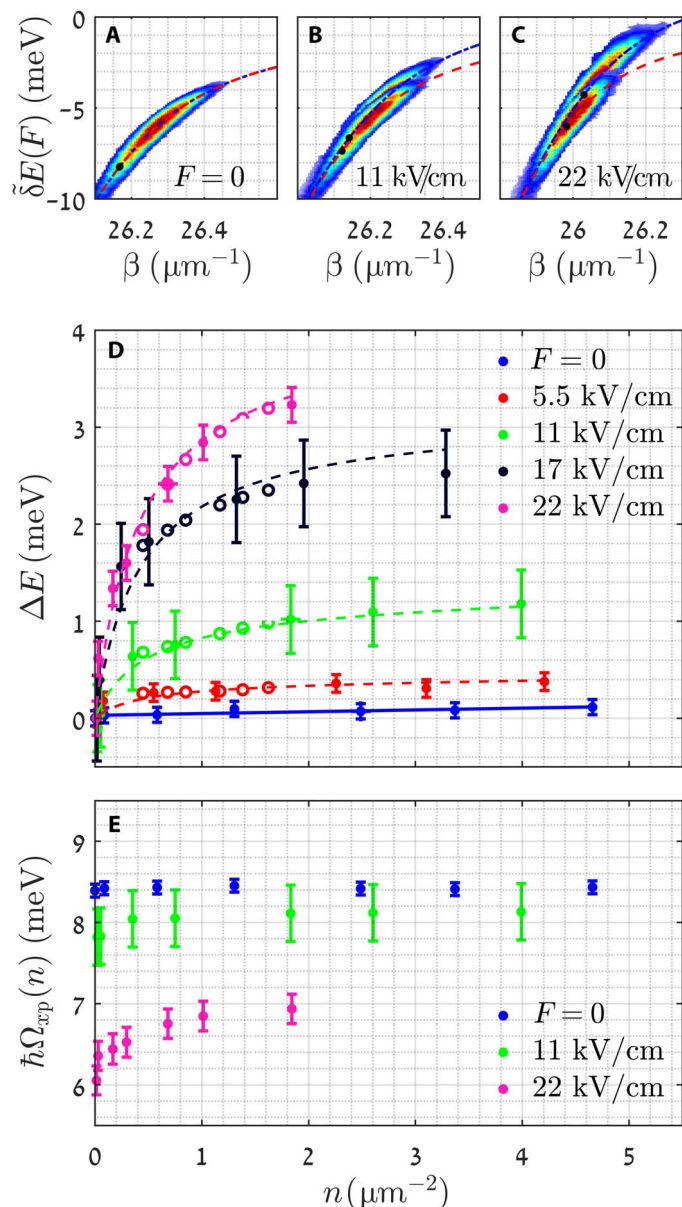


**Fig. 2. Strong dipolar interactions between polaritons.** (A to C) Overlaid polariton PL dispersions measured with low and high excitation powers under different values of  $F$ . The dashed lines are fits to the coupled oscillator model, and the black dots mark polaritons with  $\chi_x = 1/2$ . The energy blue shift, which increases with increasing electric field, is an indication for the dipolar interaction between polaritons (full separate images of all the six corresponding dispersions can be found in the Supplementary Materials). (D) Energy shift of the polariton mode as a function of the polariton density for different values of  $F$ . The solid blue line is a linear fit for the case of  $F = 0$ , and the dashed curves are the fits to the theoretical model given in the text. (E) Dependence of  $\Omega_{\text{xp}}$  on  $n$  for various values of  $F$ . An increase in  $n$  results in an energy blue shift, which, in turn, tends to increase the optical dipole moment of the exciton, leading to an increase of  $\Omega_{\text{xp}}$ . The effect is stronger as  $F$  increases.

in energy with increasing excitation power when  $F > 0$  and that this energy blue shift increases with increasing  $F$  (Fig. 2, B and C). More quantitative analysis can be acquired by fitting these measured dispersions to the mode dispersions calculated using a full electromagnetic numerical model. The comparison between the measured dispersions

and the numerically calculated ones are shown in the Supplementary Materials. Another useful analysis method is a fit to the coupled oscillator model, which describes the strong coupling between the exciton and the WG mode. These fits are shown by the dashed lines in Fig. 2 (A to C). From those fits, we extract the energy of polaritons for any given excitonic fraction,  $\chi_x$ . Energy variations of the lower polariton mode can result from two mechanisms. The first is due to exciton-exciton interactions that shift the excitonic part of the polariton and thus the whole polariton dispersion. The second is a variation in the optical coupling of the exciton to the photon (due to screening, for example), which, in turn, changes the Rabi splitting  $\hbar\Omega_{\text{xp}}$  and can also result in an apparent blue shift of the lower polariton dispersion. It is thus vital to unambiguously identify the source of the observed energy blue shift. While this identification might be nontrivial in microcavities, in WG structures, it is quite straightforward: Whereas a blue shift arising from exciton-exciton interactions is accompanied by a shift in the parallel momentum of the polariton dispersion, a blue shift that results from mere variations of  $\Omega_{\text{xp}}$  occurs without this momentum shift. Therefore, by following the variations with the polariton density of  $\beta(\chi_x = 1/2)$  (marked by the black dots in Fig. 2, A to C), one can single out the contributions of the interaction-induced blue shift of the exciton part and the contributions from variations in  $\Omega_{\text{xp}}$ , as is detailed in the Supplementary Materials. In Fig. 2D, we plot the interaction-induced blue-shift energy of the  $\chi_x = 1/2$  point of the lower polariton branch,  $\Delta E = E(n) - E(n = 0)$ , as a function of the observed polariton density  $n$ , under the outcoupler, for different values of  $F$ , and in Fig. 2E, we plot the change in  $\Omega_{\text{xp}}$  as a function of  $n$  for different values of  $F$ . The polariton density was estimated by carefully counting the photons emitted through the grating and using the proper calibration of losses and cloud size (for more details on the calibration procedure, please refer to Materials and Methods).

The case of  $F = 0$  corresponds to unpolarized polaritons, while for  $F > 0$ , the polaritons are dipolar (dipolaritons), with increasing dipole moment. This blue-shift energy is the result of polariton-polariton interactions. A small blue shift is observed for unpolarized polaritons as their density is increased (blue dots in Fig. 2D). This blue shift energy is attributed to the short-range, nondipolar polariton-polariton interactions. From the fitted linear dependence  $\Delta E = g_0 n$  (solid blue line in Fig. 2D), the interaction strength  $g_0$  can be extracted:  $g_0 = 18 \pm 8 \mu\text{eV} \mu\text{m}^2$ . This value is in the same order of magnitude of the  $g_0 = 25$  to  $37 \mu\text{eV} \mu\text{m}^2$  reported by Walker *et al.* (13) for unpolarized WG-polaritons with narrow InGaAs QWs and the  $g_x = 30 \mu\text{eV} \mu\text{m}^2$  reported by Rodriguez *et al.* (33) for pure excitons in InGaAs QW. We note that while in the studies of Walker *et al.* (13) and Rodriguez *et al.* (33) the excitation was with a continuous wave laser, as mentioned above here the excitation is pulsed and there is a spatial and temporal separation of the polariton cloud from possible reservoir excitons or charges (see Materials and Methods for more details).

A large increase of  $\Delta E$  values is observed for the cases where  $F > 0$  compared to the  $F = 0$  case. For any tested density,  $\Delta E$  is larger for larger  $F$  values. This substantial enhancement of  $\Delta E$  as  $F$  increases is attributed to the contribution of dipole-dipole interactions between dipolaritons, which, as can be seen, are much stronger than the nondipolar interactions. The reduction of  $\Omega_{\text{xp}}$  with  $F$  results from the reduction in the overlap between the wave functions of the hole and the electron as  $F$  increases (15). As  $n$  increases, we find that  $\Omega_{\text{xp}}$  also increases. This is expected as the blue shift tends to reverse the field-induced  $e$ - $h$  separation in the QW and thus  $i\Omega_{\text{xp}}$  increases. We note that we do not observe a significant reduction in  $\Omega_{\text{xp}}$  due to phase-space filling or carrier

screening (34). To verify the dipolar nature of the interactions and quantify their magnitude, we consider the dependence of  $\Delta E$  on  $F$  for a given constant density. The interaction energy in a dipolar gas is expected to be proportional both to the density of the dipoles and to their dipole length. Thus, we can expect the following expression for  $\Delta E$

$$\Delta E(d, n) = g_0 n + g_d(n) n = g_0 n + \alpha d(n) n \quad (1)$$

where  $g_d$  is the dipolar interaction strength that characterizes the dipolar interactions and  $d(n)$  is the dipole length, which also depends on  $n$  (15). By dividing Eq. 1 by  $g_0 n$ , we obtain an expression for the enhancement factor  $\eta(n, d_0)$ , which quantifies the increase in the interaction strength compared to the unpolarized case (here,  $d_0$  is the dipole length for  $n = 0$ )

$$\eta_n(d_0) = \frac{g_d(d_0, n)}{g_0} = \frac{\alpha d(d_0, n)}{g_0} \quad (2)$$

In Fig. 3A, we plot  $\eta$  as a function of  $d_0$  for three different polariton densities. We find that  $\eta$  increases linearly with  $d_0$  and that large interaction enhancement factors can be achieved, reaching almost 200 and yielding a maximal measured  $g_d \sim 2.4 \text{ meV } \mu\text{m}^2$ .

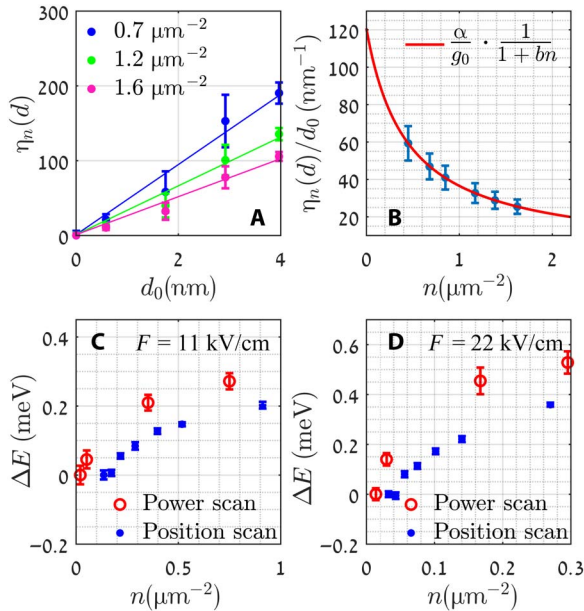


**Fig. 3. Enhancement of the polariton-polariton interactions.** (A) Interaction enhancement factor  $\eta_n(d)$  for various densities (interpolated, marked by the open circles in Fig. 2D) plotted as a function of  $d_0$ . Interaction enhancements of up to almost 200-fold are observed for the highest  $F$  values. (B) Dependence of  $\eta_n(d)/d_0$  on  $n$  fitted to the theoretical model described in the text. (C and D) Comparison between the energy shift measured with a fixed excitation distance  $\Delta X$  and an increasing excitation power (red circles) and the energy shift measured with a fixed excitation power and decreasing excitation distance  $\Delta X$  for two values of  $F$ . Here, the energy was measured at a constant  $\beta$  value [the difference in the magnitudes of  $\Delta E(\beta)$  and  $\Delta E(\chi_x = 1/2)$  is explained in the Supplementary Materials]. The similarity between the two experiments suggests that the measured energy blue shifts are a result of local polariton interactions at the readout point.

The linear dependence on the dipole length verifies the dipolar nature of the enhanced polariton-polariton interactions. Moreover, the slopes of the curves in Fig. 3A represent the magnitude  $\eta/d_0$ , from which both  $\alpha$  and  $d(n)$  can be deduced. In the Supplementary Materials, we derive a simple model, which shows that the dipole moment is expected to reduce with increasing density as  $d(n) = d_0/(1 + bn)$ , where  $b$  is a constant. In Fig. 3B, we plot the slopes as a function of  $n$  together with a fit to  $\alpha/(g_0(1 + bn))$ . We find a good agreement between the experiment and the functional form of  $d(n)$ . We deduce  $\alpha/g_0 = 122 \pm 2 \text{ nm}^{-1}$  and  $\alpha = 2.2 \pm 1.0 \text{ eV } \mu\text{m}$ . These extracted values and the above model for  $d(F, n)$  are then plugged back into Eq. 1 and are compared to the measured dependence  $\Delta E(d_0, n)$ , where a best fit is done only within their extracted error limits. The prediction of Eq. 1 fits well the experimental results, as is seen by the dashed lines in Fig. 2D. This confirms the self-consistency of our model and analysis.

### Measurements of the interaction-induced polariton scattering

These strong polariton-polariton interactions, observed through the increase of the mean energy of the polariton system, are also expected to have a strong enhancement of polariton-polariton scattering processes. Elastic scattering of polaritons should lead to a redistribution of the polariton population in momentum space (35, 36). For the case of polaritons in a WG, all having similar propagation constants along the WG direction and small quantized momenta parallel to the propagation direction, these elastic collisions should result in a significant scattering out of the guided modes into leaky, nonguided modes, and thus to additional propagation loss, as is depicted schematically in Fig. 1A. Inelastic scattering processes should lead to a redistribution of the polariton population along the dispersion. This has motivated us to look at the propagation dynamics of the dipolaritons. In Fig. 4A, we plot the measured polariton emission from the outcoupler for three different excitation distances  $\Delta X$  and three different values of  $F$ . On each plot, we show the fitted coupled oscillator model and three points, which mark the locations with specific excitonic fractions,  $\chi_x = 3/4$ ,  $\chi_x = 1/2$ , and  $\chi_x = 1/4$ , respectively. It is evident that as  $F$  increases, there is an increasing shift of the apparent polariton population toward lower energies for growing  $\Delta X$ . This indicates that the decay length of polaritons that are more excitonic is significantly shorter than that of polaritons that are more photonic and that there might be a redistribution of polaritons. This effect is negligible for the case where  $F = 0$ . These loss and redistribution of populations seem consistent with the picture of the dominant role of dipolar interactions in dynamical scattering processes. To model these dynamics, we write a rate equation for the propagating polariton population, following their initial excitation

$$\frac{\partial n}{\partial t} = -\gamma_{\text{pol}} \cdot n - \gamma_{\text{col}} \cdot n^2 \quad (3)$$

where  $\gamma_{\text{pol}}$  is the single particle loss rate and  $\gamma_{\text{col}}$  is the coefficient of collisions between two polaritons. The second term in Eq. 3 represents the loss due to polariton-polariton collisions, which, as discussed above, result in scattering outside of the guided modes and thus in loss of WG-polaritons (we exclude the possibility of a self-diffusive motion of the polaritons, as, unlike the case of polariton diffusion in slab WGs (37), here any scattering-induced in-plane momentum change that is larger than the small lateral critical angle of the WG mode would result in an in-plane scattering out of the WG and an effective loss rather than diffusive motion). When divided by the group velocity  $v_g^{\text{pol}}$ , Eq. 3 can be

rearranged to give the spatial decay along the WG. This differential equation can be solved analytically giving

$$n(x) = \frac{e^{-x/L}}{n_0^{-1} + \frac{\gamma_{\text{col}}}{\gamma_{\text{pol}}}(1 - e^{-x/L})} \quad (4)$$

Here,  $L = v_g^{\text{pol}}/\gamma_{\text{pol}}$  is the single polariton decay length and  $n_0$  is the initial density. In Fig. 4B, we plot the relative change in the total emission intensity of the polaritonic branch as a function of  $\Delta X$  for four different values of  $F$  together with the fits to Eq. 4. For  $F = 0$ , the decay fits well to an exponent, with  $\gamma_{\text{col}} \approx 0$  indicating negligible two-body collisions. The decay length decreases as  $F$  increases, and the decay becomes nonexponential. In Fig. 4C, we plot the extracted values of  $\gamma_{\text{col}}$  against

$d_0$ . It fits well to a quadratic increase with  $d_0$ , another strong indication of a dipole-dipole induced scattering (38).

## DISCUSSION AND CONCLUSIONS

We have established that dipole-dipole interactions take a dominant role in the dynamics of a WG-dipolariton system, overwhelming the short-range contact interactions of unpolarized polaritons. Surprisingly, the absolute value of  $g_d = \alpha d$  is much larger than the value expected by using mean-field models of interacting dipolar excitons and polaritons, which suggest  $\alpha = g_d/d \approx 4\pi e^2/\epsilon = 1.4 \text{ meV } \mu\text{m}$  (39–41). This is a significant discrepancy.

One possibility for these large blue shifts at the readout point is if they are carried by polaritons from the high-density regime at the excitation point without energy relaxation. However, this energy-conserving motion would imply the following scenario: As the polaritons move away from the large density zone to the low density readout area, their initially blue-shifted dispersion should red shift, but because of energy conservation, the polaritons should traverse up along the less blue-shifted dispersion curve. In contrast to this picture, in our experiment, the polaritons move down along the dispersion curve. The fact that the entire branch seems to shift is an evidence that the interactions accompany the polaritons as they fly away from the excitation point. Furthermore, the observed decay of population along the way due to dipolar scattering seems to contradict conserved energy transport. To

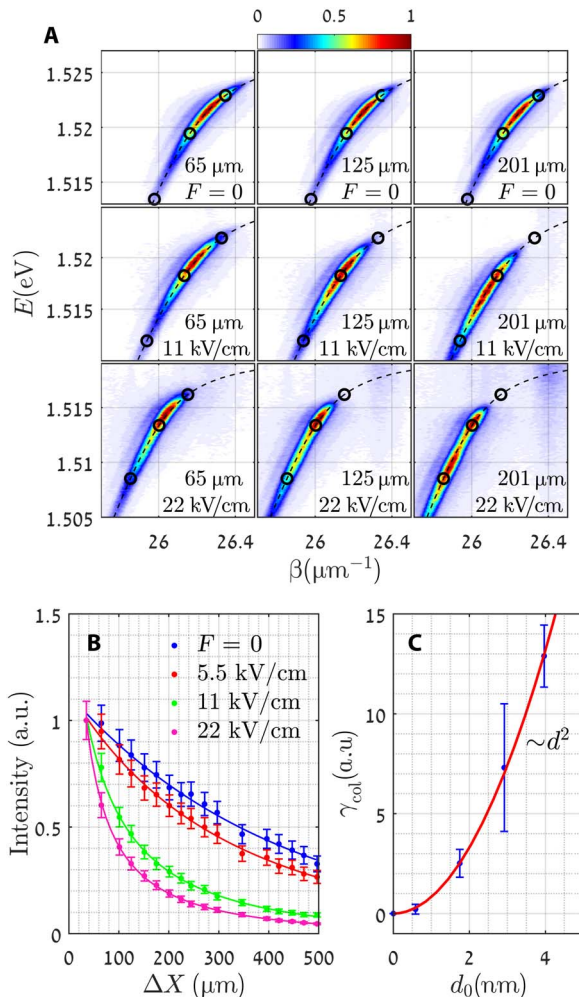


**Fig. 4. Enhanced polariton scattering.** (A) Measured dispersion from various excitation distances and different values of  $F$ . Each row represents a constant  $F$ , while each column represents a different excitation distance. The dashed lines are fits to the coupled oscillator model, and the circles represent the points in which  $\chi_x$  is  $1/4$ ,  $1/2$ , and  $3/4$ . A clear redistribution of polariton population is observed for polaritons under an applied electric field. (B) Decay of the emitted intensity with respect to the distance of excitation for different values of  $F$ . The solid lines are the fits acquired from Eq. 4. a.u., arbitrary units. (C)  $\gamma_{\text{col}}$  as a function of the dipole length together with a quadratic fit.

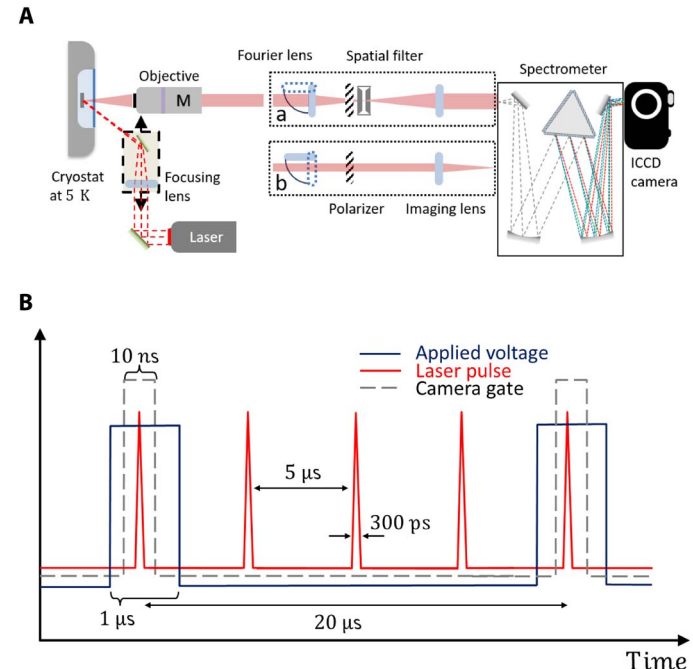


**Fig. 5. The experimental setup and the experimental timing diagram.** (A) Experimental setup. The sample is positioned inside a cold finger cryostat and kept at  $T = 5 \text{ K}$ . The sample is nonresonantly excited from the side. The emitted PL can be analyzed angularly (a) and spatially (b) by flipping the Fourier lens in and out, respectively. A spatial filter positioned at the real-space image of the Fourier lens filters out signal that originates outside of the grating area. (B) Timing diagram of the acquisition method. A 200-MHz laser excites the sample nonresonantly. The maximum trigger of the ICCD camera is 50 kHz; therefore, only one of four pulses is measured with an acquisition window of 10 ns. The voltage is applied for 1  $\mu\text{s}$ , starting 700 ns before each camera gate.

demonstrate that  $\Delta E$  results from the local density at the readout point, in Fig. 3 (C and D), we plot  $\Delta E(n)$  at the readout point for the two types of experiments (the comparison in Fig. 3 is made by following the energy change of polaritons with a specific  $\beta = \beta_a$ ). In the first experiment, we fixed the excitation power at the excitation point (and thus the density there  $n_{\text{exc}}$  and presumably  $\Delta E_{\text{exc}}$ ) and varied  $\Delta X$ . In the second experiment, we fixed  $\Delta X$  but varied the excitation power [and  $n_{\text{exc}}$  and  $\Delta E(n_{\text{exc}})$  correspondingly]. The two experiments give almost identical results. This shows that  $\Delta E$  is a result of local interactions.

Another possible explanation is the existence of a steady-state “hidden” high density of excitons or charged carriers that accumulate at the outcoupler area but do not emit. To induce the measured blue shifts, this density should be much larger than the measured polariton density, even for measurements done hundreds of micrometers away from the excitation point, and it should have lifetimes larger than 5  $\mu\text{s}$ , which is the time between excitation pulses. In addition, they should have the same density dependence on power and distance as the polaritons, to explain the similarity between the two curves in Fig. 3 (C and D), and should have a suppressed emission. These are very stringent restrictions. Alternatively, large measured  $g_d$  values might be expected if there is an enhancement of the polaritonic interactions over that of bare excitons, or if polaritons form microscopic high-density droplets, so that local densities within each droplet are much higher than the average polariton density. A droplet instability can occur through attractive dipolar interactions of dipoles in adjacent QWs. A high-density droplet formation was observed in atomic gases with magnetic dipole-dipole interactions (42–44). Future experiments with time-resolved detection are planned to further investigate these issues.

A large enhancement of the dipolar interaction of dipolaritons compared to that of unpolarized polaritons can facilitate observation of two-polariton interactions in readily achieved conventional optical confinement (in contrast to deep subwavelength optical confinement) (45, 46). We note that because there is already an optical confinement in the vertical direction and in one lateral direction due to the presence of the WG, confinement in the propagation direction of the WG mode can be achieved by different methods, for example, by adding lateral reflectors to the WG, resulting in a full lateral confinement of the polaritons.

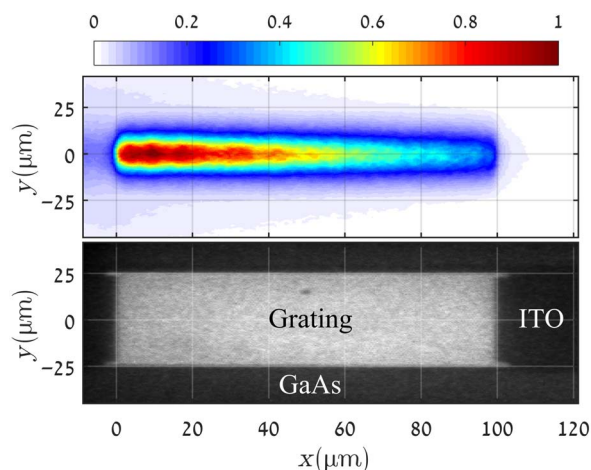


**Fig. 6. PL signal from the output grating.** An image of the grating when it is illuminated by white light (bottom) and the normalized PL along the grating, measured for  $F = 0$  (top).

This polariton blockade can be observed via second-order correlation measurements, where photon anti-bunching is expected. This blockade will be a major step toward polariton-based quantum gates.

The observed large enhancement of the polariton-polariton interactions induced by their electric dipole, together with the ability to precisely control this enhancement and effectively turn it on and off via the external bias in well-defined and selective locations via patterned electrical gates, can now allow to design complex WG structures where the interactions between polaritons can be spatially and temporally controlled. This, together with the long-range nature of dipolar interactions, might be used to construct various lattice simulations, and it is such a set of properties that was theoretically suggested for observing a new type of topological states, namely, topolaritons in WGs (22). Furthermore, the ability demonstrated here to truly guide polaritons in fully confined WGs without any complex sample etching opens up possibilities for polariton-based complex circuitry.

## MATERIALS AND METHODS

### Experimental setup

The experimental setup is illustrated in Fig. 5A. During the experiment, the sample was mounted inside a cold finger cryostat and kept at a temperature of 5 K. The optical imaging setup supported two modes of operation, which were toggled by the presence or absence of a Fourier lens: With the Fourier lens present, the Fourier plane of the collection objective was imaged on the entrance slit of the spectrometer, resulting in angular-resolved emission spectra. Furthermore, in the Fourier imaging mode, a small aperture was positioned at the first real-space image plane of the Fourier lens. The dimensions of the aperture were chosen such that only light emitted through the grating outcoupler was allowed to pass. This spatial filter allowed us to completely separate the polariton signal from emission originating from the vicinity of the remote excitation spot. In both modes of operation, the signal was filtered by a polarizer to collect only light from the transverse electric-polarized WG-polaritons [see discussion in the study of Rosenberg *et al.* (15)] and by an 800-nm long-pass filter, which block scattering of the 774.5-nm excitation source. To ensure no buildup of long-lived exciton or charge reservoirs between excitation pulses, in all experiments, the applied voltage was modulated and synchronized with the excitation pulse and the exposure window, and was turned off after every exposure until the next one. The voltage on time was 1  $\mu\text{s}$  long, starting 700 ns before the moment of optical excitation. It had an off time of 4  $\mu\text{s}$  between optical excitations, which is an ample time for the subnanosecond recombination of all excitons. Between optical pulses, during the voltage off-time, there was no field-induced charge separation and the excitons were essentially unpolarized. Figure 5B shows the timing scheme of our experiments. The procedure described above ensures both spatial and temporal separation of polaritons and excitons/charges. The separation occurs because, after the excitation pulse, the polaritons propagate very fast toward the spatially remote output grating, where their emission is being captured within the temporal window of the gated camera. The temporal width of the polariton cloud is given by the temporal width of the laser pulse, which was <300 ps. The excitons/charges move much slower from the excitation point (with typical velocities of 1 to 10  $\mu\text{m}/\text{ns}$ ) (31, 32) and could not make it to the remote output grating within 300 ps. If carriers/excitons ever reach the grating within one excitation cycle, they do that much after the polariton signal has gone, so there were no local mutual interactions between excitons/carriers and the measured polaritons originating from the same pulse.

## Calibration of the polariton density

To derive the relation between the number of photons emitted via the grating coupler and the density of the polaritons, we first used the following rate equation model for polaritons that propagate along the outcoupling

$$\frac{\partial n}{\partial t} = -\gamma n - \gamma_{\text{col}} n^2 \quad (5)$$

where  $\gamma = \gamma_r + \gamma_{\text{nr}}$  is the overall decay rate,  $\gamma_{\text{nr}}$  is the nonradiative decay along the ITO channel under the output grating, and  $\gamma_r$  is the added loss due to the outcoupling of polaritons through the grating. In Fig. 6, we plotted the spatial distribution of the emitted PL from the area of the grating for  $F = 0$ . Because the emitted intensity is given by

$$I(x) = \gamma_r n(x) \quad (6)$$

we found

$$I(x) = \frac{v_g \tilde{\gamma}_r e^{-\tilde{\gamma} x}}{n_0^{-1} + \frac{\tilde{\gamma}_{\text{col}}}{\tilde{\gamma}} (1 - e^{-\tilde{\gamma} x})} \quad (7)$$

where  $\tilde{\gamma}_r = \gamma_r / v_g$ . By integrating over the emitted intensity, we could relate the total number of emitted photons  $N_{\text{ph}}$  to the polariton density, which arrived to the grating  $n_0$  (see the Supplementary Materials for a more detailed derivation), and obtained

$$n_0 = \frac{\tilde{\gamma}}{\tilde{\gamma}_{\text{col}} (1 - e^{-\tilde{\gamma} d})} \left( e^{\frac{N_{\text{ph}} \tilde{\gamma}_{\text{col}}}{\Delta y v_g \tilde{\gamma}_r}} - 1 \right) \quad (8)$$

## Density calibration procedure

The expression in Eq. 8 is used to derive the density of the polaritons given  $t_p = 280$  ps,  $\Delta y = 17$   $\mu\text{m}$ ,  $d = 100$   $\mu\text{m}$ , and  $\tilde{\gamma}_r \sim 1/330$   $\mu\text{m}^{-1}$  (see the Supplementary Materials). The value of  $\tilde{\gamma}_{\text{col}}$  is the same as the one calculated by fitting to Eq. 4. The group velocity,  $v_g$ , which is the mean velocity of the polaritons, was extracted from the fits to the coupled oscillator model. From those fits, the population at each excitonic fraction  $\chi_x(\beta)$  [or photonic fraction  $\chi_{\text{ph}}(\beta)$ ] is found, from which the mean polaritonic fractions and the mean velocity are extracted.  $N_{\text{ph}}$  is acquired from the counts of the ICCD, where we used the following calibration routine: First, we quantified the loss of the optical setup, using a laser beam traversing along the whole optical path of the system and measuring the relative transmitted power at the CCD (yielding a transmission of 0.4). Then, we directly measured the conversion between counts on the ICCD to incident photons. Using the above procedure, we extracted the conversion between photons entering the measurement system to counts on the ICCD. In addition, we also used a finite-difference time-domain simulation of the optical WG mode propagation under the output grating to find the ratio between the number of photons that are emitted toward the objective side to the number of photons that are emitted toward the substrate side. We found this ratio to be roughly unity, which adds a factor of 2 to the conversion between ICCD counts to polaritons. Because the angular emission spread from the sample (in the  $y$  direction, perpendicular to the WG-polariton propagation direction) is  $\sim 30^\circ$ , while the effective optical acceptance of the setup (limited by the slit of the spectrometer in the Fourier configuration) lets only  $0.73^\circ$  in, we multiplied the counts to polariton conversion factor by  $31/0.73 \approx 42$ .

## SUPPLEMENTARY MATERIALS

Supplementary material for this article is available at <http://advances.sciencemag.org/cgi/content/full/4/10/eaat8880/DC1>

Supplementary Text

Fig. S1. Raw images of the PL dispersion spectral measurements used to create Fig. 1C.

Fig. S2. Raw images of the PL dispersion spectral measurements used to create Fig. 2 (A to C).

Fig. S3. The effect of the energy of the exciton on the polariton energy.

Fig. S4. The decay of the emission intensity along the grating coupler.

Fig. S5. The temporal shape of the laser pulse, measured with a Streak camera.

Fig. S6. Illustration of the two mechanisms, which can blue shift the energy of the polariton.

## REFERENCES AND NOTES

1. A. Imamoglu, R. J. Ram, Quantum dynamics of exciton lasers. *Phys. Lett. A* **214**, 193–198 (1996).
2. L. S. Dang, D. Heger, R. André, F. Boeuf, R. Romestain, Stimulation of polariton photoluminescence in semiconductor microcavity. *Phys. Rev. Lett.* **81**, 3920–3923 (1998).
3. P. Senellart, J. Bloch, Nonlinear emission of microcavity polaritons in the low density regime. *Phys. Rev. Lett.* **82**, 1233–1236 (1999).
4. J. Kasprzak, M. Richard, S. Kundermann, A. Baas, P. Jeambrun, J. M. J. Keeling, F. M. Marchetti, M. H. Szymańska, R. André, J. L. Staehli, V. Savona, P. B. Littlewood, B. Deveaud, L. S. Dang, Bose-Einstein condensation of exciton polaritons. *Nature* **443**, 409–414 (2006).
5. R. Balili, V. Hartwell, D. Snoke, L. Pfeiffer, K. West, Bose-Einstein condensation of microcavity polaritons in a trap. *Science* **316**, 1007 (2007).
6. K. G. Lagoudakis, M. Wouters, M. Richard, A. Baas, I. Carusotto, R. André, L. S. Dang, B. Deveaud-Plédran, Quantized vortices in an exciton-polariton condensate. *Nat. Phys.* **4**, 706–710 (2008).
7. G. Roumpos, M. D. Fraser, A. Löffler, S. Höfling, A. Forchel, Y. Yamamoto, Single vortex-antivortex pair in an exciton-polariton condensate. *Nat. Phys.* **7**, 129–133 (2011).
8. S. Utsunomiya, L. Tian, G. Roumpos, C. W. Lai, N. Kumada, T. Fujisawa, M. Kuwata-Gonokami, A. Löffler, S. Höfling, A. Forchel, Y. Yamamoto, Observation of Bogoliubov excitations in exciton-polariton condensates. *Nat. Phys.* **4**, 700–705 (2008).
9. A. Amo, D. Sanvitto, F. P. Laussy, D. Ballarini, E. del Valle, M. D. Martin, A. Lemaître, J. Bloch, D. N. Krizhanovskii, M. S. Skolnick, C. Tejedor, L. Viña, Collective fluid dynamics of a polariton condensate in a semiconductor microcavity. *Nature* **457**, 291–295 (2009).
10. S. Kim, B. Zhang, Z. Wang, J. Fischer, S. Brodbeck, M. Kamp, C. Schneider, S. Höfling, H. Deng, Coherent polariton laser. *Phys. Rev. X* **6**, 011026 (2016).
11. M. J. Hartmann, Quantum simulation with interacting photons. *J. Opt.* **18**, 104005 (2016).
12. A. Amo, J. Bloch, Exciton-polaritons in lattices: A non-linear photonic simulator. *C. R. Phys.* **17**, 934–945 (2016).
13. P. Walker, L. Tinkler, B. Royall, D. V. Skryabin, I. Farrer, D. A. Ritchie, M. S. Skolnick, D. N. Krizhanovskii, Dark solitons in high velocity waveguide polariton fluids. *Phys. Rev. Lett.* **119**, 097403 (2017).
14. P. M. Walker, L. Tinkler, D. V. Skryabin, A. Yulin, B. Royall, I. Farrer, D. A. Ritchie, M. S. Skolnick, D. N. Krizhanovskii, Ultra-low-power hybrid light-matter solitons. *Nat. Commun.* **6**, 8317 (2015).
15. I. Rosenberg, Y. Mazuz-Harpaz, R. Rapaport, K. West, L. Pfeiffer, Electrically controlled mutual interactions of flying waveguide dipolaritons. *Phys. Rev. B* **93**, 195151 (2016).
16. J. Ciers, J. G. Roch, J.-F. Carlin, G. Jacopin, R. Butté, N. Grandjean, Propagating polaritons in III-nitride slab waveguides. *Phys. Rev. Appl.* **7**, 034019 (2017).
17. M. Saffman, T. G. Walker, K. Mølmer, Quantum information with Rydberg atoms. *Rev. Mod. Phys.* **82**, 2313–2363 (2010).
18. M. Saffman, Quantum computing with atomic qubits and Rydberg interactions: Progress and challenges. *J. Phys. B* **49**, 202001 (2016).
19. H. Gorniaczyk, C. Tresp, J. Schmidt, H. Fedder, S. Hofferberth, Single-photon transistor mediated by interstate Rydberg interactions. *Phys. Rev. Lett.* **113**, 053601 (2014).
20. H. Kübler, J. P. Shaffer, T. Baluktsian, R. Löw, T. Pfau, Coherent excitation of Rydberg atoms in micrometre-sized atomic vapour cells. *Nat. Photonics* **4**, 112–116 (2010).
21. H. Weimer, M. Müller, I. Lesanovsky, P. Zoller, H. P. Büchler, A Rydberg quantum simulator. *Nat. Phys.* **6**, 382–388 (2010).
22. T. Karzig, C.-E. Bardyn, N. H. Lindner, G. Refael, Topological polaritons. *Phys. Rev. X* **5**, 031001 (2015).
23. Y. Sun, Y. Yoon, M. Steger, G. Liu, L. N. Pfeiffer, K. West, D. W. Snoke, K. A. Nelson, Direct measurement of polariton-polariton interaction strength. *Nat. Phys.* **13**, 870–875 (2017).
24. Y. Shilo, K. Cohen, B. Laikhtman, K. West, L. Pfeiffer, R. Rapaport, Particle correlations and evidence for dark state condensation in a cold dipolar exciton fluid. *Nat. Commun.* **4**, 2335 (2013).
25. K. Cohen, Y. Shilo, K. West, L. Pfeiffer, R. Rapaport, Dark high density dipolar liquid of excitons. *Nano Lett.* **16**, 3726–3731 (2016).

26. M. Stern, V. Umansky, I. Bar-Joseph, Exciton liquid in coupled quantum wells. *Science* **343**, 55–57 (2014).
27. A. A. High, E. E. Novitskaya, L. V. Butov, M. Hanson, A. C. Gossard, Control of exciton fluxes in an excitonic integrated circuit. *Science* **321**, 229–231 (2008).
28. G. J. Schinner, J. Repp, E. Schubert, A. K. Rai, D. Reuter, A. D. Wieck, A. O. Govorov, A. W. Holleitner, J. P. Kotthaus, Confinement and interaction of single indirect excitons in a voltage-controlled trap formed inside double InGaAs quantum wells. *Phys. Rev. Lett.* **110**, 127403 (2013).
29. P. Cristofolini, G. Christmann, S. I. Tsintzos, G. Deligeorgis, G. Konstantinidis, Z. Hatzopoulos, P. G. Savvidis, J. J. Baumberg, Coupling quantum tunneling with cavity photons. *Science* **336**, 704–707 (2012).
30. G. Bastard, E. E. Mendez, L. L. Chang, L. Esaki, Variational calculations on a quantum well in an electric field. *Phys. Rev. B* **28**, 3241–3245 (1983).
31. D. Snoke, S. Denev, Y. Liu, L. Pfeiffer, K. West, Long-range transport in excitonic dark states in coupled quantum wells. *Nature* **418**, 754–757 (2002).
32. A. Gärtner, A. W. Holleitner, J. P. Kotthaus, D. Schuh, Drift mobility of long-living excitons in coupled GaAs quantum wells. *Appl. Phys. Lett.* **89**, 052108 (2006).
33. S. R. K. Rodriguez, A. Amo, I. Sagnes, L. Le Gratiet, E. Galopin, A. Lemaitre, J. Bloch, Interaction-induced hopping phase in driven-dissipative coupled photonic microcavities. *Nat. Commun.* **7**, 11887 (2016).
34. D. Huang, J.-I. Chyi, H. Morkoç, Carrier effects on the excitonic absorption in GaAs quantum-well structures: Phase-space filling. *Phys. Rev. B* **42**, 5147–5153 (1990).
35. P. G. Savvidis, C. Ciuti, J. J. Baumberg, D. M. Whittaker, M. S. Skolnick, J. S. Roberts, Off-branch polaritons and multiple scattering in semiconductor microcavities. *Phys. Rev. B* **64**, 075311 (2001).
36. C. Ciuti, P. Schwendimann, A. Quattropani, Theory of polariton parametric interactions in semiconductor microcavities. *Semicond. Sci. Technol.* **18**, S279 (2003).
37. D. A. Zaitsev, N. D. Il'yanskaya, A. V. Koudinov, N. K. Poletaev, E. V. Nikitina, A. Yu. Egorov, A. V. Kavokin, R. P. Seisyan, Diffusive propagation of exciton-polaritons through thin crystal slabs. *Sci. Rep.* **5**, 11474 (2015).
38. J. L. Bohn, M. Cavagnero, C. Ticknor, Quasi-universal dipolar scattering in cold and ultracold gases. *New J. Phys.* **11**, 055039 (2009).
39. B. Laikhtman, R. Rapaport, Exciton correlations in coupled quantum wells and their luminescence blue shift. *Phys. Rev. B* **80**, 195313 (2009).
40. A. V. Nalitov, D. D. Solnyshkov, N. A. Gippius, G. Malpuech, Voltage control of the spin-dependent interaction constants of dipolaritons and its application to optical parametric oscillators. *Phys. Rev. B* **90**, 235304 (2014).
41. O. Kyriienko, E. B. Magnusson, I. A. Shelykh, Spin dynamics of cold exciton condensates. *Phys. Rev. B* **86**, 115324 (2012).
42. H. Kadau, M. Schmitt, M. Wenzel, C. Wink, T. Maier, I. Ferrier-Barbut, T. Pfau, Observing the Rosensweig instability of a quantum ferrofluid. *Nature* **530**, 194–197 (2016).
43. I. Ferrier-Barbut, H. Kadau, M. Schmitt, M. Wenzel, T. Pfau, Observation of quantum droplets in a strongly dipolar Bose gas. *Phys. Rev. Lett.* **116**, 215301 (2016).
44. L. Chomaz, S. Baier, D. Petter, M. J. Mark, F. Wächtler, L. Santos, F. Ferlaino, Quantum-fluctuation-driven crossover from a dilute Bose-Einstein condensate to a macrodroplet in a dipolar quantum fluid. *Phys. Rev. X* **6**, 041039 (2016).
45. A. Verger, C. Ciuti, I. Carusotto, Polariton quantum blockade in a photonic dot. *Phys. Rev. B* **73**, 193306 (2006).
46. O. Kyriienko, I. A. Shelykh, T. C. H. Liew, Tunable single-photon emission from dipolaritons. *Phys. Rev. A* **90**, 033807 (2014).

#### Acknowledgments

**Funding:** The work at the Hebrew University had a financial support from the U.S. Department of Energy, Office of Basic Energy Sciences, Division of Materials Sciences and Engineering; the United States–Israel Binational Science Foundation (BSF grant 2016112); and the Israeli Science Foundation (grant no. 1319/12). The work at Princeton University was funded by the Gordon and Betty Moore Foundation through EPIQS initiative grant GBMF4420 and by NSF MRSEC grant DMR-1420541. **Author contributions:** K.W. and L.P. epitaxially grew the sample. I.R. performed all the postgrowth fabrications. I.R. and R.R. conceived the project. I.R. and D.L. built the experimental setup. I.R. did the measurements. I.R. and R.R. performed the analysis. I.R., D.L., and Y.M.-H. were responsible for the numerical simulations. **Competing interests:** The authors declare that they have no competing interests. **Data and materials availability:** All data needed to evaluate the conclusions in the paper are present in the paper and/or the Supplementary Materials. Additional data related to this paper may be requested from the authors.

Submitted 16 April 2018

Accepted 10 September 2018

Published 19 October 2018

10.1126/sciadv.aat8880

**Citation:** I. Rosenberg, D. Liran, Y. Mazuz-Harpaz, K. West, L. Pfeiffer, R. Rapaport, Strongly interacting dipolar-polaritons. *Sci. Adv.* **4**, eaat8880 (2018).